HHS Public Access

Author manuscript

ACS Nano. Author manuscript; available in PMC 2019 September 16.

Published in final edited form as:

ACS Nano. 2019 August 27; 13(8): 9620–9628. doi:10.1021/acsnano.9b04783.

Hydrogel-coated microneedle arrays for minimally-invasive sampling and sensing of specific circulating nucleic acids from skin interstitial fluid.

Dana Al Sulaiman[†,#], **Jason Y. H. Chang**[‡,#], **Nitasha R. Bennett**[‡], **Helena Topouzi**[†], **Claire A. Higgins**[†], **Darrell J. Irvine**[‡,¥,¶,Φ,§,*], **Sylvain Ladame**[†,*]

[†]Department of Bioengineering, Imperial College London, London SW7 2AZ, U.K.

[‡]Koch Institute for Integrative Cancer Research, Massachusetts Institute of Technology, Cambridge, MA 02139, U.S.A.

[¥]Department of Materials Science and Engineering, Massachusetts Institute of Technology, Cambridge, MA 02139, U.S.A.

[¶]Department of Biological Engineering, Massachusetts Institute of Technology, Cambridge, MA 02139, U.S.A.

[Φ]Ragon Institute of MIT, MGH, and Harvard, Boston MA 02139.

[§]Howard Hughes Medical Institute, 4000 Jones Bridge Rd., Chevy Chase, MD.

Abstract

Minimally-invasive technologies that can sample and detect cell-free nucleic acid biomarkers from liquid biopsies have recently emerged as clinically useful for early diagnosis of a broad range of pathologies, including cancer. Although blood has been so far the most commonly interrogated body fluid, skin interstitial fluid has been mostly overlooked despite containing the same broad variety of molecular biomarkers originating from cells and surrounding blood capillaries. Minimally-invasive technologies have emerged as a method to sample this fluid in a pain-free manner and often take the form of microneedle patches. Herein, we developed microneedles that are coated with an alginate-peptide nucleic acid hybrid material for sequence-specific sampling, isolation and detection of nucleic acid biomarkers from skin interstitial fluid. Characterized by fast sampling kinetics and large sampling capacity (~6.5μL in 2 min), this platform technology also enables for the first time the detection of specific nucleic acid biomarkers either on the patch itself or in solution after light-triggered release from the hydrogel. Considering the emergence of cell-free nucleic acids in bodily fluids as clinically informative biomarkers, platform technologies that can detect them in an automated and minimally invasive fashion have great potential for personalized diagnosis and longitudinal monitoring of patient-specific disease progression.

[*]**Corresponding Author:** s.ladame@imperial.ac.uk, djirvine@mit.edu.
[#]These authors contributed equally.

Supporting Information.
The following files are available free of charge.
Experimental procedures for the chemical and physical characterization of the PNA and PNA-alginate hydrogels (PDF)

Keywords

microneedle; hydrogel; skin interstitial fluid; microRNA; biomarker

Liquid biopsies have the potential to revolutionize the way patients are screened, treated and monitored, all of which are key drivers of precision medicine.[1–4] Although affordable full genome sequencing may help identify individuals at risk of developing specific pathologies, snapshots provided by point-of-care testing through simple technologies that are both low-cost and highly automated remain essential for public screening or personalized longitudinal monitoring. Circulating, cell-free nucleic acids (cfNAs) in liquid biopsies have been reported as predictive, diagnostic and prognostic biomarkers for a broad range of conditions, most notably cancer.[5–8] Among them microRNAs (or miRs),[9–14] a class of non-coding RNAs 19–25 nucleotides in length, hold the greatest promise as either individual biomarkers or in combinations.[15–19] Hence, there is a growing demand for sensing technologies that can detect specific nucleic acids in biological fluids and that can be implemented in the clinic. Research on cfNAs has so far been limited almost exclusively to those found in blood or urine.[20–23] However, recent experimental evidence suggests that all species of RNA (including miRs) previously found in blood are also present, in similar proportions, within interstitial fluid (ISF)[24] validating this type of bodily fluid as a greatly overlooked source of biomarkers for personalized medicine. Surrounding cells within a tissue, ISF serves as an exchange medium between blood plasma and cells and contains a combination of molecular constituents found in both sources. Skin ISF is found within several hundred microns of the skin surface, primarily in the connective tissue dermis where only few capillary beds and pain receptors reside. It can therefore be sampled in a pain-free manner, without any risk of blood contamination. This contrasts with blood drawing techniques that can be invasive (venous blood) or result in poor quality samples (fingerstick capillary blood).

Minimally-invasive technologies for skin ISF sampling have emerged that are based on compact patches of microneedles (MNs).[25–34] They are typically made of an array of microscale solid, porous or hollow needles from materials such as glass, metal, silicon or other polymers.[35–36] Hollow needles were designed to create pathways for ISF extraction via capillary force or vacuum-induced suction. They represent very useful alternatives to invasive sampling technologies traditionally based on micro-dialysis and requiring tubing implantation under local anesthetics. Current limitations of many of the MN patches engineered so far include low sampling capacity (<2 μL) and/or long sampling times (e.g. > 1h to sample enough ISF volumes for subsequent biomarker analysis). In addition, to the best of our knowledge, there has been no report of MNs engineered to sample and detect specific nucleic acid biomarkers from skin ISF. So far, MN were at best used for sampling and releasing total skin ISF and circulating nucleic acids detected after heavy sample processing and PCR-based analysis.[37]

Herein, we report the first example of hydrogel-coated MN patches that can sample and isolate specific miRNA biomarkers from skin ISF at the fastest rate yet while enabling the captured miRNA to be detected in situ (Figure 1a). Our versatile platform also offers the capability of light-triggered release of the miRNA for post-sampling off-chip analysis. Poly-

L-Lactide (PLLA) arrays of 77 microneedles were chosen as our sampling platform as we previously reported their successful use for either transdermal vaccine delivery or ISF/cell sampling from the skin.[38–44]

RESULTS AND DISCUSSION

7 × 7 mm arrays were produced as previously reported by us that were decorated with pyramidal-shaped MNs (Figure S1). The height of the needles was set to 550 μm to enable them to penetrate through the epidermis layer and reach the underlying, ISF containing, dermis layer. For sampling and isolation of specific miRNA biomarkers from skin ISF, the MN array was coated with alginate polymers functionalized with Peptide Nucleic Acid (PNA) capture probes for sequence-specific immobilization of the only miRNA of interest via Watson-Crick base pairing. When compared to standard oligonucleotides, PNAs offer the advantage of a greater affinity and sequence-specificity when hybridizing to complementary DNA or RNA strands.[45–49] Accessible through easily scalable solid-phase peptide synthesis, PNAs have proven highly valuable analytical tools for nucleic acid sensing, both in vitro and in vivo, and are particularly well suited for the detection of short oligonucleotides such as miRNAs.[50–53] Herein, a 7-mer PNA (of sequence GACACGC) was designed that was complementary to the 5'-end of miR-210 ($^{5'}$CUGUGCGUGUGACAGCGGCUGA$^{3'}$), a recently identified biomarker for early systemic melanoma recurrence and chosen as a model system for our proof-of-concept study (Figure S2). the Melanoma patients with abnormally elevated levels of circulating miR-210 were indeed found to be more likely to have disease recurrence, reinforcing the need for a non-invasive test suitable for longitudinal monitoring.[54–55] Throughout this proof-of-concept study, a DNA version of miR-210 (DNA-210, $^{5'}$CTGTGCGTGTGACAGCGGCTGA$^{3'}$) was chosen as our target of interest.

The PNA capture probe (Figure S2) was functionalized at its C-terminus with an alkyne moiety to facilitate its covalent immobilization to an azide-modified alginate via copper-catalyzed cycloaddition reaction (click chemistry). A photo-cleavable linker (3-Amino-3-(2-nitrophenyl) propanoic acid) (PCL) was also introduced between the alkyne and the PNA sequence to enable the release of the PNA:DNA hybridization complex post ISF sampling via photo-activation with near-UV light (300–360nm) (Figure 1a). PNA length of 7-mer was chosen to allow stable PNA:DNA or PNA:RNA heteroduplex formation at human body temperature (melting temperature T_m > 37°C), as previously reported.[56]

The alginate-azide polymer was prepared as previously reported by EDC/NHS mediated peptide coupling between low viscosity alginate and 11-azido-3,6,9-trioxyundecan-1-amine (Figure S3), leading to an average level of azide functionalization of 17 mol% (Figure S5).[57] The alginate-PNA hybrid material was finally assembled by azide-alkyne cycloaddition reaction, in the presence of Cu(II) sulphate, Tris[(1-benzyl-1H-1,2,3-triazol-4-yl)methyl]amine (TBTA) and sodium ascorbate (Figure S4), leading to an overall level of PNA functionalization of 1 mol% as assessed by ^{1}H-NMR spectroscopy (Figure S5).

Coating of the MN arrays with the newly engineered alginate-PNA proceeded in three steps: pre-coating with poly-L-Lysine followed by deposition of the alginate and finally physical

crosslinking with calcium chloride ($CaCl_2$), leaving enough time for the MN to dry between each step. Once fully dried, scanning electron microscopy (SEM) was used to characterize and compare the physical morphology at the surface of the MN patches with and without alginate-PNA hydrogel coating (Figure 1b). To determine the effect of PNA functionalization on the alginate's physical properties, MN patches coated with unmodified alginate were also analyzed. The SEM micrographs of both types of alginate displayed an interconnected network of pores with a relatively consistent pore size. Although SEM does only provide information on the hydrogels' structures in their non-swollen dehydrated form, it is noteworthy that the average pore size of the dehydrated alginate-PNA coating however was approximately half that of the unmodified alginate (Figure S6). This could be due to the hydrophobic nature of these charge-free PNAs limiting water uptake and reducing swelling, as previously observed when functionalizing hydrogel fibers with hydrophobic moieties.[58] Atomic Force Microscopy (AFM) was also used to gain an insight into the topography of the alginate-PNA on surface. For ease of imaging however, the hydrogel was deposited on a glass slide but this time no lyophilization or metal coating was needed, therefore providing a more accurate representation of the hydrogel structure. The surface topography showed a relatively consistent and homogeneously distributed porous structure over the 50×50 μm^2 area with pores or voids of 200–800nm (Figure S7), only slightly larger than those observed, after lyophilization, by SEM. As earlier studies from our group showed, small oligonucleotides the size of miRNAs could easily diffuse within such porous materials and hybridize to pre-embedded PNAs.[59]

The main limitations of existing ISF sampling platforms are their low sampling capacity and low sampling rates. For example, micro-dialysis techniques typically sample at 1–5 μL/min while less invasive capillary ultrafiltration is even slower, at 100–150 nL/min. The swelling behavior of our hydrogel-coated MNs was assessed in buffer (PBS) and at physiological body temperature (37°C). Figure 1d describes the volume of liquid absorbed by the MN over time which can be fitted by the Spring and Dashpot Voight-based model commonly used for describing swelling kinetics of hydrogels. According to this model, the hydrogel-coated MNs have an equilibrium swelling capacity of 6.5 ± 0.2 μL, with a sampling rate constant of 0.74, meaning that 63% of the full swelling capacity is achieved in less than 1 min. This compares very favorably with other recently reported hydrogel-coated MN sampling technologies and can at least in part be attributed to the large surface area of the MNs due their pyramidal shape and porous coating structure.

To test the ability of our MN patches to sample and isolate nucleic acids in a sequence specific manner, MNs were dipped into solutions (100 μL) containing various amounts of DNA-210 (0–500 nM) labelled with Alexa 647 dye. After 15 min sampling, the MNs were washed thoroughly with water and dried overnight at room temperature before imaging with a fluorescence scanner (Typhoon FLA9500, GE Healthcare). As shown in Figure 2a, a plot of the mean fluorescence intensity (N=22 individual microneedles from 2 different MN patches) versus DNA concentration demonstrates the ability of our patches to detect target concentrations as low as ~6 nM, with a linear regime across almost 2 orders of magnitude (6–500 nM). Sequence specificity was then confirmed by demonstrating the statistically significant ability of the MN patch to discriminate between a complementary and a non-complementary DNA target, both labelled with the same fluorophore (Figure 2b).

In order to demonstrate the possibility to release the captured nucleic acid from the microneedle, MN patches pre-incubated with fluorescently-labelled DNA-210 were placed tips-down in water (100 μL) within a UV crosslinker (UVP) and irradiated with increasing amounts of UV energy (λex= 315 nm, 0–4 J/cm^2). After shaking for 1 h, the MNs were rinsed, dried and imaged on a fluorescence scanner. A significant loss in fluorescence intensity of the MN was observed post-irradiation that suggested the release of over 70% of the captured DNA after 1 min of irradiation (Figure S8).

Our MN patches were not only designed to sample specific endogenous nucleic acid biomarkers from skin ISF but also to enable their quantitative detection once sampled. Two different mechanisms for sensing were explored that involved either (i) the direct visualization of the isolated biomarker whilst captured on the microneedle patch or (ii) an alternative two-step process involving light-triggered release of the PNA:DNA complex followed by detection in solution (Figure 2c). For both sensing strategies, the MN patches were initially dipped into solutions (100 μL) containing various amounts of unlabeled DNA-210 (10–200 nM), then washed thoroughly to remove any unbound DNA and dried. For direct visualization, the MN patches were then incubated in a solution of DNA intercalator (SYBR Safe, 2X concentration, Invitrogen), washed and imaged with a fluorescence scanner (Figure 2d). For indirect visualization, the DNA-loaded MN were then placed tips-down into 100 μL of water and photo-irradiated for 3 min at 3 J/cm^2 in a photo-crosslinker (BLX-315, λex = 315 nm). A solution of DNA intercalator was then added to detect the PNA:DNA duplex released in solution (Figure 2e). Both strategies proved successful at detecting nM concentrations of nucleic acids sampled with our MN patches, highlighting the versatility of this platform. Whilst simpler and more direct on-chip detection is perfectly suited for applications that require testing at the point-of-care, the possibility of releasing the captured and purified (i.e. separated from all other ISF constituents, including other nucleic acid) material offer the option to detect and sequence less abundant biomarkers (through amplification-based methodologies). It is noteworthy however, that both detection approaches are mutually complementary and could even potentially be carried out sequentially.

Having validated the sensitivity and selectivity of the MN sampling in vitro, we sought to investigate the sampling of specific nucleic acids from skin ISF directly in human skin, using an ex-vivo model. Human abdominal skin samples were first prepared by incubation with either a complementary (DNA-210) or a non-complementary (DNA-141) oligonucleotide labelled with Alexa-647 dye (500 nM each) and then washed thoroughly with water. MN patches were then pressed onto the skin surface (15 min, 37°C) for sampling and then washed extensively and dried overnight before fluorescence imaging (Figure 3a). Images were analyzed by taking the average fluorescence of individual microneedles on each patch (N = 48 microneedles from three different MN patches). These results not only demonstrate that our MNs can indeed sample nucleic acids from skin ISF but also that they retain their high sequence specificity, capturing preferentially (15-fold) the DNA fragment complementary to the PNA incorporated into the hydrogel (Figure 3b).

To confirm these findings a second experiment was prepared where the skin samples were incubated in a solution containing a mixture of both DNA-210 (red bars) and DNA-141

(green bars) labelled with Alexa-647 and 6-FAM, respectively. After sampling (as described above), MN patches (N = 3 per condition) were imaged successively under two excitation filters (Figure 3c). Whilst no significant difference between the experiments with and without DNA was detectable with the Cy2 filter (for 6-FAM visualization), a very strong signal increase was observed between the DNA-free control and the experiment with DNA, confirming the efficient and sequence-specific capturing of DNA-210 spiked within human skin ISF. Fluorescent confocal imaging of the MNs was also performed to confirm the previous findings and visualize the DNA captured around each MN (Figure 3d). Non-complementary DNA-141 imaged with 488ex/510em showed little to no fluorescence signal on the MNs (Figure 3d, left), while complementary DNA-210 imaged with 647ex/665em showed fluorescence signal bound to the MN (Figure 3d, middle). A 3D projection of the fluorescence signal from a single microneedle is also shown (Figure 3d, right).

CONCLUSION

In summary, we have developed a new generation of MN patches coated with hybrid alginate-PNA hydrogels that can sample up to 6.5 μL of fluid in 2 minutes. Unlike other sampling technologies reported to date, we demonstrated that attaching PNA oligomers to the hydrogel's fibers also enables the specific sampling, purification and release of the only nucleic acid fragments that are complementary to the PNA sequence. This versatile platform can therefore by easily tuned by simply adapting the PNA sequence to that of any miRNA of interest. Functionalization of the hydrogel with different PNA sequences complementary to different miRNAs is also currently underway in our labs, that will also enable the sampling and sensing of multiple miRNAs simultaneously (known as multiplexed analysis or profiling). Optical sensing of the captured biomarkers is also possible, either directly on-chip or in-solution after an additional light-triggered release step. Using a human skin ex-vivo model, we also demonstrated that this technology could efficiently capture nucleic acids spiked within skin interstitial fluids with both high efficiency and sequence specificity. With the recent experimental evidence that skin ISF contains the same RNA species (including circulating miRNAs) as blood with comparable natural abundance, minimally-invasive technologies that can not only sample this body fluid but can also interrogate its composition have the potential to transform the field of molecular diagnostics from liquid biopsies.

EXPERIMENTAL METHODS

Solid Phase PNA Synthesis:

PNA probe directed against miR-210 was designed to contain an alkyne group (C-terminus) for ease of attachment to the alginate hydrogel fibers as well as a photosensitive group for ease of release by UV irradiation after sampling. The 7-mer PNA oligomer (Figure S2) was synthesized via standard Solid Phase Peptide Synthesis (SPPS) exploiting the chemistry of 9-fluoromethoxycarbonyl (Fmoc) protecting groups.

Synthesis of Alginate-PNA conjugates:

Alginate was functionalized with azide groups via peptide bond formation following a protocol adapted from Breger *et al.* (Figure S3).[60] Briefly, a 1 wt% solution of alginate was

prepared by dissolving 500 mg of alginate (low viscosity alginate from brown algae, ~100,000 g/mol Sigma) in 50 mL of MES buffer (50 mM, pH 4.0). To this solution, the following was added sequentially: 20 mM *N*-ethyl-*N'*-(3-dimethylamino-propyl) carbodiimide hydrochloride (EDC·HCl, Sigma), 140 mM *N*-hydroxysuccinimide (NHS, Sigma), and 1.8 mL of 11-azido-3,6,9-trioxaundecan-1-amine (AA, SelectLab 134179-38-7). The reaction was set at RT overnight with constant stirring. The reaction mixture was next dialyzed (MWCO 12 kDa) against aqueous NaCl for 1 day then against ddH_2O for three days. Finally, the purified product was lyophilized to produce a white product, which was characterized by ^{1}H-NMR (D_2O, 400 MHz, 363 K).

Alginate-azide was functionalized with PNA-alkyne via a copper-catalyzed azide–alkyne cycloaddition reaction (Click chemistry) as adapted from Presolski *et al.*[57] Briefly, a 1 wt% solution of alginate-azide was prepared in 100 mM phosphate buffer (pH = 7.4). To this solution, PNA-alkyne was added at an amount equivalent to 1 mol% (i.e. 8.1 mg PNA-alkyne per 100 mg alginate-azide). Next, copper (II) sulphate ($CuSO_4$, Sigma) and the ligand Tris[(1-benzyl-1*H*-1,2,3-triazol-4-yl)methyl]amine (TBTA, Sigma) were mixed together then added to the reaction solution to produce a final concentration of 0.1 mM $CuSO_4$ and 0.5 mM TBTA. Finally, sodium ascorbate (Sigma) was added to the solution at a final concentration of 5 mM. The reaction vessel was then sealed and left to react at RT overnight. After 24 h, the reaction solution was diluted 5 times, and the reaction was left to proceed for a further 24 h. To chelate and remove copper (II) ions from the solution, 10 mM Ethylenediamine tetraacetic acid (EDTA, Sigma) was added before the entire solution was dialyzed against ddH_2O for three days, lyophilized, and characterized by ^{1}H-NMR (D_2O, 400 MHz, 363 K).

Preparation of Hydrogel-coated Microneedles:

Poly-L-Lactide (PLLA; RESOMER L 207 S, Evonik Industries AG) MNs were prepared as previously reported by us.[38] The dimensions of the MN patch can be seen in Figure S1. It is noteworthy that the height of the MN patch, which is 0.55 mm or 550 microns, was designed to allow the needles to penetrate the epidermis layer (100–200 microns) and reach the underlying dermis layer, containing a rich source of IF. The bare MNs were functionalized with an engineered hydrogel coating via a three-step coating procedure based on a protocol developed by Mandal *et al.*[38] Firstly, 50 μL of a 0.01 wt% solution of positively-charged poly-L-lysine (150,000–300,000 g/mol, Sigma-Aldrich, P4832) was pipetted onto each MN to form an adsorbed layer that will subsequently facilitate electrostatic adhesion of the alginate hydrogel. The solution was removed after 30 min, and the MNs were left to dry under a fume hood at RT for at least 1 h. Secondly, 60 μL of alginate solution, composed of 0.35 mg alginate-PNA and 1.4 mg sucrose (Sigma) in 60 μL ddH_2O, was pipetted onto each MN array. The MNs were then left to dry under a fume hood at RT for at least 3 h. Finally, 50 μL of crosslinking solution, composed of 20 mM $CaCl_2$ (Sigma), was pipetted onto each MN, after which the coated arrays were left to dry at RT overnight (>12h).

Sampling Protocol:

To visualize the captured DNA after MN sampling, fluorescently-labeled (Alexa-647, unless otherwise indicated) single stranded target DNA-210 (as a proxy for miRNA-210) and non-

target DNA-141 (as a proxy for miR-141) were purchased from Invitrogen. For sampling, single MN patches were placed tips-down into individual wells of a clear 48-well microplate (Corning, half-area) filled with 100 μL of analyte solution. The solution consisted of either water/buffer (control), target DNA-210 or non-target DNA-141 at concentrations indicated for each experiment. After sampling at 37°C for 15 min (unless otherwise indicated), the MNs were removed, washed thoroughly with ddH_2O (10 min, 3 washes) then imaged by a fluorescence scanner (Typhoon FLA 9500, PMT 300V, 25 μm pixel resolution, λex = 635 nm unless otherwise indicated). Images were analyzed by Fiji (Image J) software to quantify fluorescence intensity.

DNA Release Protocol:

To release or recover captured NA after sampling, MN patches were placed tips-down into individual wells of a clear 48-well microplate (Corning, half-area) filled with 100 μL of ddH_2O. Next, the plate was inserted into a UV-crosslinker (BLX-315 crosslinker, 315 nm, Consort) and irradiated with amounts of UV energy as indicated by each experiment to break off the PNA:DNA duplex. After 1h of shaking (250 RPM, RT), the MNs were removed from the wells, rinsed and dried overnight. In the case when DNA was labelled with Alexa-647 dye, the MNs were imaged after release to show loss of fluorescence, equivalent to release of DNA (Typhoon FLA 9500, PMT 300V, 25 μm pixel resolution, λex=635 nm). In the case when DNA was unlabeled, thiazole orange (TO, 2 μM) was added to the solution in each well and kept for 30 min before imaging with a plate reader (Omega, λex=488 nm, λem=520 nm, gain=1000).

Preparation of Human Skin Samples:

Human abdominal skin with adipose tissue was purchased from Caltag medsystems (Buckingham, U.K.). The sample was washed in Dulbecco's minimal essential medium (DMEM; Gibco Life Technologies) supplemented with 2% Antimycotic-Antibiotic (ABAM; Gibco Life Technologies) for 30 min. Then, it was moved to DMEM supplemented with 1% ABAM for the rest of the procedure. Using sterile surgical scissors, subcutaneous fat was removed in order to obtain only the epidermis with the dermis. A series of 8 mm2 area punches were made using a biopsy punch (Stiefel) to create nine skin samples (N=3 replicates per condition) for the following MN sampling experiment.

MN Application to Human Skin:

MNs were pressed onto human skin samples by a gentle thumb press. After 15 min at 37°C, MNs were gently removed. To show penetration, skin was stained with trypan blue (0.4% diluted in half by ddH_2O, sterile-filtered, Sigma, T8154). After 10 min, skin samples were rinsed thoroughly then imaged by a wide field microscope under bright field illumination to show a characteristic MN penetration pattern.

MN Sampling from Skin:

Just before sampling with MNs, skin samples were removed from the culture media (DMEM with 1% ABAM) then washed thoroughly with ddH_2O (three times). To load the skin with DNA, the samples were gently transferred to 48-well microplates and placed on top of 100

μL solutions containing either: ddH_2O (control), 500 nM non-target DNA-141, or 500 nM target DNA-210, where both DNA fragments were labelled with Alexa-647 dye (N=3 samples per condition). Skin samples were left to incubate on the solutions overnight in the fridge. On the next day, the samples were carefully removed from the incubation solutions with sterile tweezers, rinsed thoroughly with ddH_2O, then placed in a 48-well microplate. For the MN sampling experiment, single MN patches were gently pressed onto each skin sample by a gentle thumb press, and the MNs were left to sample at 37°C for 15 min. Next, the MNs were gently removed from the skin, rinsed thoroughly (ddH_2O, three times) and left to dry overnight before being imaged with a fluorescence scanner (Typhoon FLA 9500, PMT 400V, 25 μm pixel resolution, λex = 635 nm, Cy5 setting). A second experiment was conducted exactly as the first described above but wherein skin samples were left to incubate on a solution containing a mixture of DNA: target DNA-210 tagged with Alexa-647 and non-target DNA-141 tagged with fluorescein, both at 500 nM. The rest of the experiment was prepared as outlined above but the MNs were imaged after sampling at two wavelengths: 635 nm (Cy5 setting) to image the target DNA-210 and 473 nm (Cy2 setting) to image the non-target DNA-141.

It is important to note that when incubating the skin samples in the solutions containing fluorescently-labelled DNA, the samples were floating on the surface with the bottom dermis layer of the skin in contact with the solution. Molecules from the solution could not cross the intact and highly impermeable stratum corneum from the top. Thus, after sampling the skin with MNs, any fluorescence signal detected on the MN originated from molecules which have diffused from solution through the dermis and into the epidermis.

Supplementary Material

Refer to Web version on PubMed Central for supplementary material.

ACKNOWLEDGMENT

This work was supported in part by an Imperial College London Ph.D. scholarship (D.A.S.), and a Fellowship supported by the S. Leslie Misrock Frontier Research Fund for Cancer Nanotechnology at the Koch Institute for Integrative Cancer Research at MIT (J.Y.H.C). S.L. also acknowledges funding from a Cancer research U.K. project grant (C49996/A26141). This work was supported in part by the U. S. Army Research Laboratory and the U. S. Army Research Office through the Institute for Soldier Nanotechnologies, under contract number W911NF-13-D-0001. We thank Drs. Chensu Wang, and Leyuan Ma for the technical assistance and Dr. Hannah Watkins for helpful discussions regarding microneedle characterization. We thank the Koch Institute Swanson Biotechnology Center for technical support, specifically David Mankus for helping with SEM imaging of microneedle arrays (Nanotechnology Materials Core Facility). D.J.I. is an investigator of the Howard Hughes Medical Institute.

REFERENCES

(1). Siravegna G; Marsoni S; Siena S; Bardelli A Integrating liquid biopsies into the management of cancer. Nat. Rev. Clin. Oncol 2017, 14, 531–548. [PubMed: 28252003]

(2). Crowley E; Di Nicolantonio F; Loupakis F; Bardelli A Liquid biopsy: monitoring cancer-genetics in the blood. Nat. Rev. Clin. Oncol 2013, 10, 472–484. [PubMed: 23836314]

(3). Ono S; Lam S; Nagahara M; Hoon DSB Circulating microRNA biomarkers as liquid biopsy for cancer patients: pros and cons of current assays. J. Clin. Med 2015, 4, 1890–1907. [PubMed: 26512704]

(4). Brock G; Castellanos-Rizaldos E; Hu L; Coticchia C; Skog J Liquid biopsy for cancer screening, patient stratification and monitoring. Transl. Cancer Res 2015, 4, 280–290.

(5). Rainer TH; Lam NYL Circulating nucleic acids and critical illness. Ann. N. Y. Acad. Sci 2006, 1075, 271–277. [PubMed: 17108220]

(6). Fleischhacker M; Schmidt B Circulating nucleic acids (CNAs) and cancer-a survey. Biochim. Biophys. Acta 2007, 1775, 181–232. [PubMed: 17137717]

(7). Swarup V; Rajeswari MR Circulating (cell-free) nucleic acids – a promising, non-invasive tool for early detection of several human diseases. FEBS Lett 2007, 581, 795–799. [PubMed: 17289032]

(8). Danese E; Montagnana M; Fava C; Guidi GC Circulating nucleic acids and hemostasis: biological basis behind their relationship and technical issues in assessment. Semin. Thromb. Hemost 2014, 40, 766–773. [PubMed: 25173499]

(9). Bartel DP MicroRNAs: genomics, biogenesis, mechanism, and function. Cell 2004, 116, 281–297. [PubMed: 14744438]

(10). Ambros V The functions of animal microRNAs. Nature 2004, 431, 350–355. [PubMed: 15372042]

(11). Meltzer PS Cancer genomics: Small RNAs with big impacts. Nature 2005, 435, 745–746 (2005). [PubMed: 15944682]

(12). Saito Y; Jones PA Epigenetic activation of tumor suppressor microRNAs in human cancer cells. Cell Cycle 2006, 5, 2220–2222. [PubMed: 17012846]

(13). Croce CM Causes and consequences of microRNA dysregulation in cancer. Nat. Rev. Genet 2009, 10, 704–714. [PubMed: 19763153]

(14). Cho WCS MicroRNAs: potential biomarkers for cancer diagnosis, prognosis and targets for therapy. Int. J. Biochem. Cell Biol 2010, 42, 1273–1281. [PubMed: 20026422]

(15). Lu J; Getz G; Miska EA; Alvarez-Saavedra E; Lamb J; Peck D; Sweet-Cordero A; Ebert BL; Mak RH; Ferrando AA; Downing JR; Jacks T; Horvitz HR; Golub TR MicroRNA expression profiles classify human cancers. Nature 2005, 435, 834–838. [PubMed: 15944708]

(16). Volinia S; Galasso M; Sana ME; Wise TF; Palatini J; Huebner K; Croce CM Breast cancer signatures for invasiveness and prognosis defined by deep sequencing of microRNA. Proc. Nat. Acad. Sci. USA 2012, 109, 3024–3029. [PubMed: 22315424]

(17). Sita-Lumsden A; Dart DA; Waxman J; Bevan C Circulating microRNAs as potential new biomarkers for prostate cancer. Br. J. Cancer 2013, 108, 1925–1930. [PubMed: 23632485]

(18). Ulivi P; Zoli W miRNAs as non-invasive biomarkers for lung cancer diagnosis. Molecules 2014, 19, 8220. [PubMed: 24941344]

(19). Halvorsen AR; Helland Å; Gromov P; Wielenga VT; Talman MM; Brunner N; Sandhu V; Børresen-Dale AL; Gromova I; Haakensen VD Profiling of microRNAs in tumor interstitial fluid of breast tumors – a novel resource to identify biomarkers for prognostic classification and detection of cancer. Mol. Oncol 2017, 11, 220–234. [PubMed: 28145100]

(20). Weber JA; Baxter DH; Zhang S; Huang DY; Huang KH; Lee MJ; Galas DJ; Wang K The microRNA spectrum in 12 body fluids. Clin. Chem 2010, 56, 1733–1741. [PubMed: 20847327]

(21). Chen X; Ba Y; Ma L; Cai X; Yin Y; Wang K; Guo J; Zhang Y; Chen J; Guo X; Li Q; Li X; Wang W; Zhang Y; Wang J; Jiang X; Xiang Y; Xu C; Zheng P; Zhang J et al. Characterization of microRNAs in serum: a novel class of biomarkers for diagnosis of cancer and other diseases. Cell Res 2008, 18, 997–1006. [PubMed: 18766170]

(22). Chan AK; Chiu RW; Lo YD Cell-free nucleic acids in plasma, serum and urine: a new tool in molecular diagnosis. Ann. Clin. Biochem 2003, 40, 122–130. [PubMed: 12662399]

(23). Bryzgunova OE; Skvortsova TE; Kolesnikova EV; Starikov AV; Rykova EY; Vlassov VV; Laktionov PP Isolation and comparative study of cell-free nucleic acids from human urine. Ann. N. Y. Acad. Sci 2006, 1075, 334–340. [PubMed: 17108229]

(24). Miller PR; Taylor RM; Tran BQ; Boyd G; Glaros T; Chavez VH; Krishnakumar R; Sinha A; Poorey K; Williams KP; Branda SS; Baca JT; Polsky R Extraction and biomolecular analysis of dermal interstitial fluid collected with hollow microneedles. Commun. Biol 2018, 1, 173. [PubMed: 30374463]

(25). Kolluru C; Williams M; Chae J; Prausnitz MR Recruitment and collection of dermal interstitial fluid using a microneedle patch. Adv. Healthc. Mater 2019, 8, e1801262. [PubMed: 30609270]

(26). Samant PP; Prausnitz MR Mechanisms of sampling interstitial fluid from skin using a microneedle patch. Proc. Natl Acad. Sci. U.S.A 2018, 115, 4583–4588. [PubMed: 29666252]

(27). Miller PR; Narayan RJ; Polsky R Microneedle-based sensors for medical diagnosis. J. Mater. Chem. B 2016, 4, 1379–1383.

(28). Ventrelli L; Marsilio Strambini L; Barillaro G Microneedles for transdermal biosensing: current picture and future direction. Adv. Healthc. Mat 2015, 4, 2606–2640.

(29). Chua B; Desai SP; Tierney MJ; Tamada JA; Jina AN Effect of microneedles shape on skin penetration and minimally invasive continuous glucose monitoring in vivo. Sens. Actuators A Phys 2013, 203, 373–381.

(30). Ito Y; Inagaki Y; Kobuchi S; Takada K; Sakaeda T Therapeutic drug monitoring of vancomycin in dermal interstitial fluid using dissolving microneedles. Inter. J. Med. Sci 2016, 13, 271.

(31). Mukerjee EV; Collins SD; Isseroff RR; Smith RL Microneedle array for transdermal biological fluid extraction and in situ analysis. Sens. Actuators A Phys 2004, 114, 267–275.

(32). Wang PM; Cornwell M; Prausnitz MR Minimally invasive extraction of dermal interstitial fluid for glucose monitoring using microneedles. Diabetes Technol. Ther 2005, 7, 131–141. [PubMed: 15738711]

(33). Caffarel-Salvador E; Brady AJ; Eltayib E; Meng T; Alonso-Vicente A; Gonzalez-Vazquez P; Torrisi BM; Vicente-Perez EM; Mooney K; Jones DS; Bell SE; McCoy CP; McCarthy HO; McElnay JC; Donnelly RF Hydrogel-Forming Microneedle Arrays Allow Detection of Drugs and Glucose In Vivo: Potential for Use in Diagnosis and Therapeutic Drug Monitoring. PLoS One 2015, 10, e0145644. [PubMed: 26717198]

(34). Donnelly RF; Mooney K; McCrudden MT; Vicente-Pérez EM; Belaid L; González-Vázquez P; McElnay JC; Woolfson AD Hydrogel-forming microneedles increase in volume during swelling in skin, but skin barrier function recovery is unaffected. J. Pharm. Sci 2014, 103, 1478–1486. [PubMed: 24633895]

(35). Romanyuk AV; Zvezdin VN; Samant P; Grenader MI; Zemlyanova M; Prausnitz MR Collection of analytes from microneedle patches. Anal. Chem 2014, 86, 10520–10523. [PubMed: 25367229]

(36). Liu L; Kai H; Nagamine K; Ogawa Y; Nishizawa M Porous polymer microneedles with interconnecting microchannels for rapid fluid transport. RSC Adv 2016, 6, 48630–48635.

(37). Smith RL; Collins SD; Duy J; Minogue TD Silicon microneedle array for minimally invasive human health monitoring. Proc. SPIE 2018, 10491.

(38). Mandal A; Boopathy AV; Lam LKW; Moynihan KD; Welch ME; Bennett NR; Turvey ME; Thai N; Van JH; Love JC; Hammond PT; Irvine DJ Cell and fluid sampling microneedle patches for monitoring skin-resident immunity. Sci. Transl. Med 2018, 10, eaar2227. [PubMed: 30429353]

(39). DeMuth PC; Su X; Samuel RE; Hammond PT; Irvine DJ Nano-layered microneedles for transcutaneous delivery of polymer nanoparticles and plasmid DNA. Adv. Mater 2010, 22, 4851–4856. [PubMed: 20859938]

(40). DeMuth PC; Moon JJ; Suh H; Hammond PT; Irvine DJ Releasable layer-by-layer assembly of stabilized lipid nanocapsules on microneedles for enhanced transcutaneous vaccine delivery. ACS Nano 2012, 6, 8041–8051. [PubMed: 22920601]

(41). DeMuth PC; Li AV; Abbink P; Liu J; Li H; Stanley KA; Smith KM; Lavine CL; Seaman MS; Kramer JA; Miller AD; Abraham W; Suh H; Elkhader J; Hammond PT; Barouch DH; Irvine DJ Vaccine delivery with microneedle skin patches in nonhuman primates. Nat. Biotechnol 2013, 31, 1082.

(42). DeMuth PC; Garcia-Beltran WF; Ai-Ling ML; Hammond PT; Irvine DJ Composite dissolving microneedles for coordinated control of antigen and adjuvant delivery kinetics in transcutaneous vaccination. Adv. Funct. Mater 2013, 23, 161–172. [PubMed: 23503923]

(43). DeMuth PC; Min Y; Huang B; Kramer JA; Miller AD; Barouch DH; Hammond PT; Irvine DJ Polymer multilayer tattooing for enhanced DNA vaccination. Nat. Mater 2013, 12, 367. [PubMed: 23353628]

(44). DeMuth PC; Min Y; Irvine DJ; Hammond PT Implantable silk composite microneedles for programmable vaccine release kinetics and enhanced immunogenicity in transcutaneous immunization. Adv. Healthc. Mater 2014, 3, 47–58. [PubMed: 23847143]

(45). Bakhtiar R Peptide nucleic acids: deoxyribonucleic acid mimics with a peptide backbone. Biochem. Educ 1998, 26, 277–280.

(46). Shakeel S; Karim S; Ali A Peptide nucleic acid (PNA) — a review. J. Chem. Technol. Biotechnol 2006, 81, 892–899.

(47). Egholm M; Buchardt O; Christensen L; Behrens C; Freier SM; Driver DA; Berg RH; Kim SK; Norden B; Nielsen PE PNA hybridizes to complementary oligonucleotides obeying the Watson-Crick hydrogen-bonding rules. Nature 1993, 365, 566–568. [PubMed: 7692304]

(48). Demidov VV; Potaman VN; Frank-Kamenetskii MD; Egholm M; Buchard O; Sönnichsen SH; Nielsen PE Stability of peptide nucleic acids in human serum and cellular extracts. Biochem. Pharmacol 1994, 48, 1310–1313. [PubMed: 7945427]

(49). Nielsen PE; Egholm M An introduction to peptide nucleic acid. Curr. Issues Mol. Biol 1999, 1, 89–104. [PubMed: 11475704]

(50). Ryoo SR; Lee J; Yeo J; Na HK; Kim YK; Jang H; Lee JH; Han SW; Lee Y; Kim VN; Min DH Quantitative and multiplexed microRNA sensing in living cells based on peptide nucleic acid and nano graphene oxide (PANGO). ACS Nano 2013, 7, 5882–5891. [PubMed: 23767402]

(51). Gorska K; Winssinger N Rapid miRNA imaging in cells using fluorogenic templated Staudinger reaction between PNA-based probes. Methods Mol Biol 2014, 1050, 179–192. [PubMed: 24297360]

(52). Metcalf GA; Shibakawa A; Patel H; Sita-Lumsden A; Zivi A; Rama N; Bevan CL; Ladame S Amplification-Free Detection of Circulating microRNA Biomarkers from Body Fluids Based on Fluorogenic Oligonucleotide-Templated Reaction between Engineered Peptide Nucleic Acid Probes: Application to Prostate Cancer Diagnosis. Anal. Chem 2016, 88, 8091–8098. [PubMed: 27498854]

(53). Sayers J; Payne RJ; Winssinger N Peptide nucleic acid-templated selenocystine-selenoester ligation enables rapid miRNA detection. Chem. Sci 2017, 9, 896–903. [PubMed: 29629156]

(54). Ono S; Oyama T; Lam S; Chong K; Foshag LJ; Hoon DS A direct plasma assay of circulating microRNA-210 of hypoxia can identify early systemic metastasis recurrence in melanoma patients. Oncotarget 2015, 6, 7053–7064. [PubMed: 25749524]

(55). Huang SK; Hoon DS Liquid biopsy utility for the surveillance of cutaneous malignant melanoma patients. Mol. Oncol 2016, 10, 450–463. [PubMed: 26778792]

(56). Amato F; Tomaiuolo R; Nici F; Borbone N; Elce A; Catalanotti B; D'Errico S; Morgillo CM; De Rosa G; Mayol L; Piccialli G; Oliviero G; Castaldo G Exploitation of a very small peptide nucleic acid as a new inhibitor of miR-509–3p involved in the regulation of cystic fibrosis disease-gene expression. Biomed Res Int 2014, 2014, 610718 [PubMed: 24829907]

(57). Presolski SI; Hong VP; Finn MG Copper-catalyzed azide–alkyne click chemistry for bioconjugation. Curr. Protoc. Chem. Biol 2011, 3, 153–162. [PubMed: 22844652]

(58). Al Sulaiman D; Cadinu P; Ivanov AP; Edel JB; Ladame S Chemically Modified Hydrogel-Filled Nanopores: A Tunable Platform for Single-Molecule Sensing. Nano Lett 2018, 18, 6084–6093. [PubMed: 30105906]

(59). Al Sulaiman D; Chang JY; Ladame S Subnanomolar detection of oligonucleotides through templated fluorogenic reaction in hydrogels: controlling diffusion to improve sensitivity. Angew. Chem. Int. Ed 2017, 56, 5247–5251.

(60). Breger JC; Fisher B; Samy R; Pollack S; Wang NS; Isayeva I Synthesis of "click" alginate hydrogel capsules and comparison of their stability, water swelling, and diffusion properties with that of Ca(+2) crosslinked alginate capsules. J. Biomed. Mat. Res. B Appl. Biomat 2015, 103, 1120–1132.

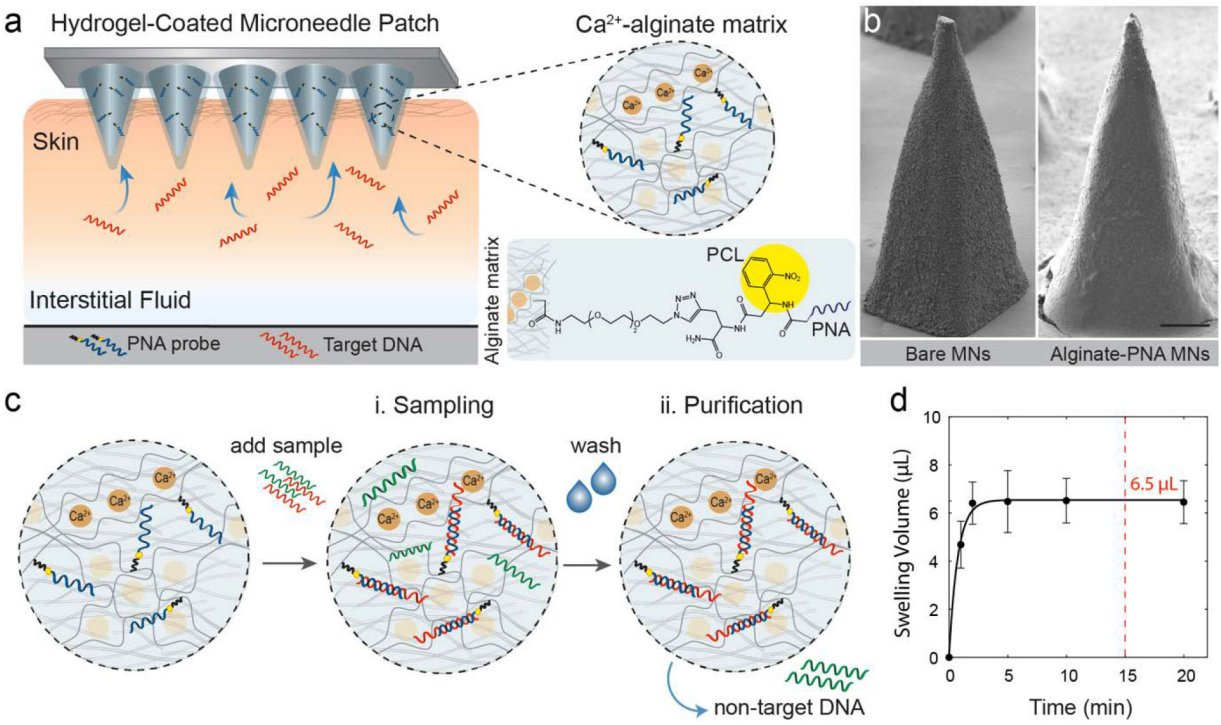

Figure 1. Schematic representation of the hydrogel-coated microneedle platform during sampling of the interstitial fluid.

(a) Microneedle arrays (MN) are functionalized with bespoke peptide nucleic acid (PNA) probes (blue) which are covalently bound to an alginate hydrogel matrix via a photo-cleavable linker (PCL, yellow). Minimally-invasive sampling of skin interstitial fluid can be achieved by pressing the coated MN patch onto the skin for 15min. (b) Scanning electron micrograph (5.0 kV, 100× magnification, 10 nm gold sputter coating) of the bare MNs and alginate-PNA hydrogel coated MNs (scale bar = 100 μm). (c) Schematic illustration of the generic protocol for MN sampling of target biomarker (red) and purification to remove non-target sequences (green). Circles represent a magnification of the alginate hydrogel coating on the MN patches. (i) When the MN is applied to sample a solution containing DNA, the target DNA sequence (red) hybridizes to the PNA probe (blue), forming a PNA:DNA duplex. (ii) The MNs are washed to remove any non-specific molecules (green) which have diffused into the hydrogel matrix. (d) Swelling kinetics of the hydrogel MNs fitted by the Spring and Dashpot Voight-based model (black solid line), showing an equilibrium swelling capacity of 6.5 ± 0.2 μL and a sampling rate constant of 0.74. Error bars show S.E.M. (N=6 MN patches).

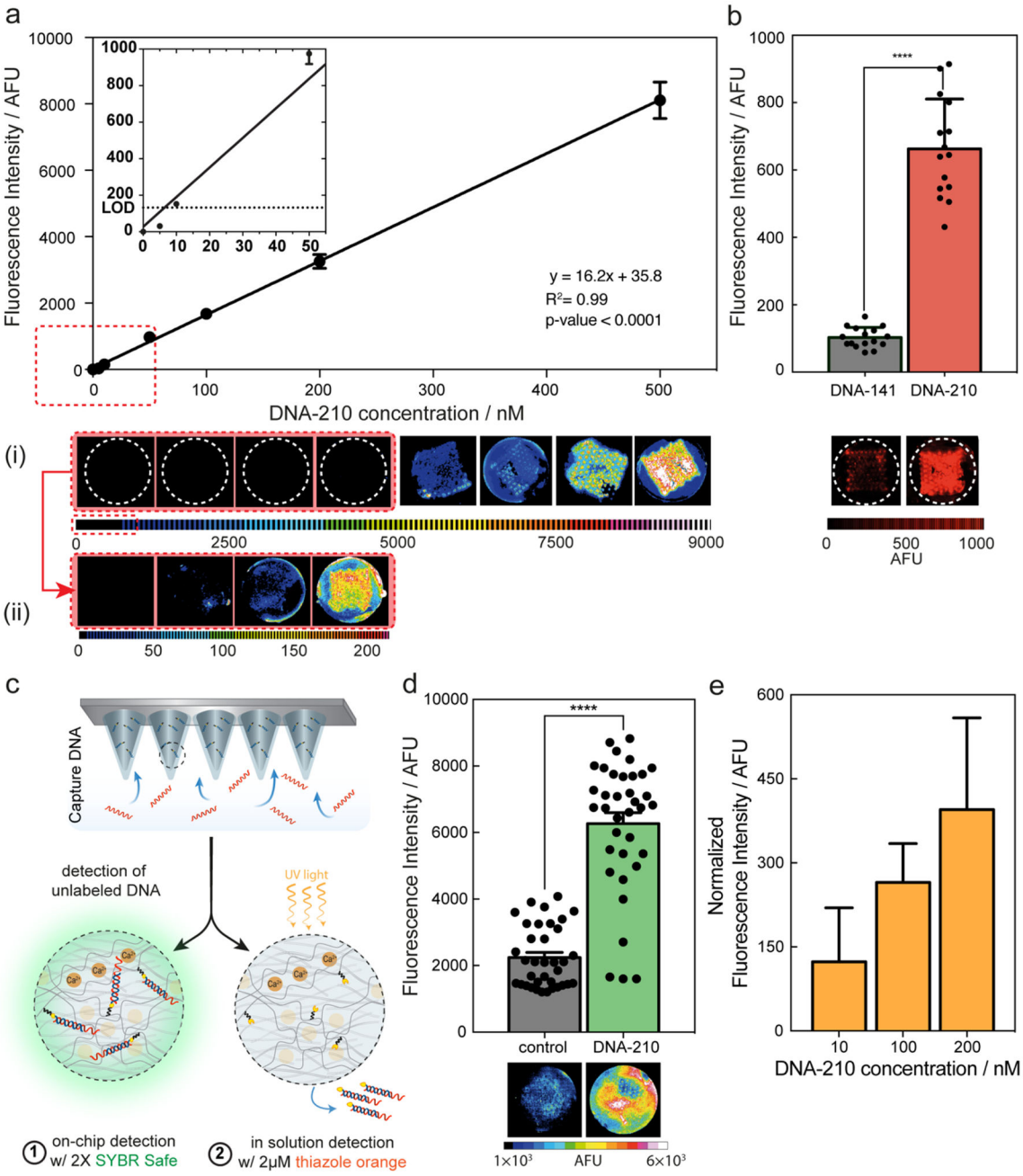

Figure 2. Validation of the MN sampling and release mechanism.

(a) Calibration curve showing the mean fluorescence intensity of N=22 needles from two MN patches (error bars show S.E.M.), with a linear regression fitting and associated equation with fitting R^2 and p-value. Fluorescence scanner images of representative MN patches after sampling fluorescently-labelled target DNA-210 at given concentrations (0–500 nM). Two color scale/calibration bars were used to facilitate visualization of the large dynamic range of fluorescence values (a (i) and a (ii), respectively). Inset shows magnification of the boxed area in (a) with the y-intercept (y-int) of the calibration curve and the limit of detection (LOD), calculated as three times the standard deviation of the y-int,

equivalent to 6 nM. (b) Specificity of MN Platform. Comparison of the mean fluorescence of N=16 needles from 2 MN patches after sampling 500 nM of non-complementary DNA-141 (left, grey) and complementary DNA-210 (right, red), with fluorescence scans of representative MN patches shown below. (c) Schematic representation illustrating the two mechanisms for detecting captured unlabeled DNA, either (1) on-chip by dipping the MN into intercalator dye to visualize the PNA:DNA duplex directly on the MN patch, or (2) by releasing the PNA:DNA duplex into solution (UV irradiation) then adding an intercalator dye to the solution. On-chip detection results are plotted in (d) showing a significant difference in fluorescence between MN sampling DNA-210 (500 nM) or control (no DNA target in 100 mM phosphate buffer, pH 7.4) (unpaired two-tailed t-test, $p<0.0001$). UV-cleaved PNA:DNA duplex detection in solution results are plotted in (e) showing an increase in fluorescence of the release solution after sampling target DNA-210 at 10, 100, or 200 nM. Note that data is normalized by subtracting the background fluorescence of the dye (2 μM, control i.e. no DNA).

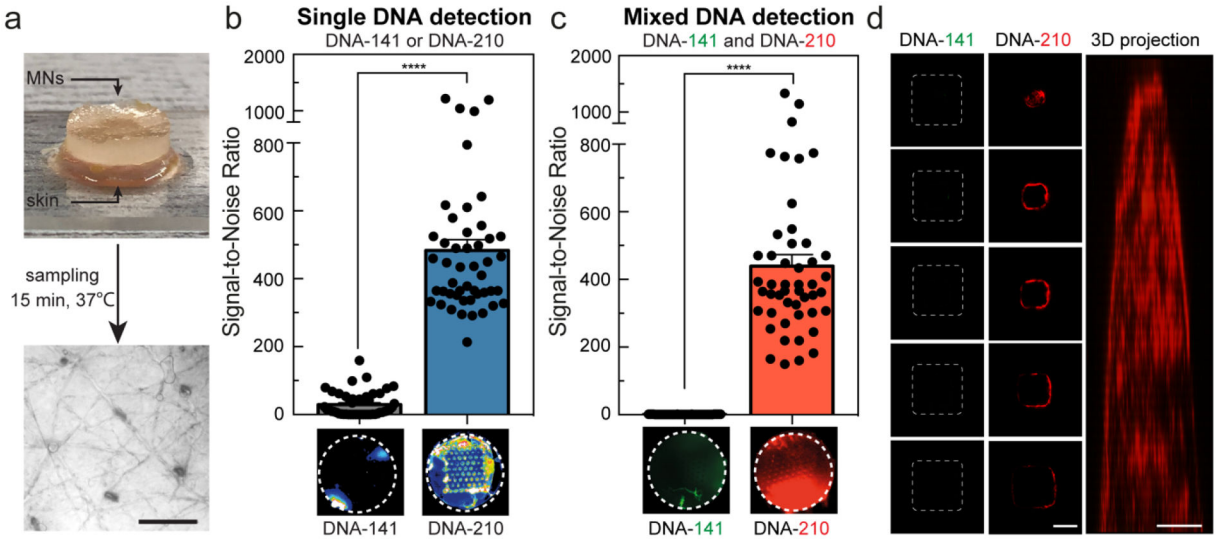

Figure 3. MN Validation with human skin sample.

(a) Experimental protocol for applying MNs to human skin biopsies. (Top) MNs were applied to 8mm2 human skin biopsies for 15 min at 37°C to sample target and non-complementary DNA. (Bottom) Optical micrograph of human skin showing MNs penetration pattern stained with trypan blue (scale bar = 300μm). SNR is represented as the ratio between average fluorescence intensity of MNs after sampling skin with DNA and without DNA (i.e. control) (N=48 from three MN patches). (b) Bars depict the SNRs after sampling skin incubated with only non-complementary DNA-141 (left, grey) or only complementary DNA-210 (right, blue), both tagged with Alexa-647 dye. (c) Bars depict the SNRs after sampling skin incubated with a mixture of complementary DNA-210 with a Cy5 dye and non-complementary DNA-210 with a Cy2 dye, imaged under Cy2 filter (left, grey) and Cy5 filter (right, red). In (b) and (c) Statistical analysis shows a significant difference between sampling target and non-complementary DNA (unpaired two-tailed t-test, p-value <0.0001). Representative MN fluorescence scans are displayed below. (d) Representative fluorescent confocal images from the captured DNA bound to the MN are shown in these images. (Left) Non-complementary DNA-141 imaged with 488ex/510em shows little to no fluorescence signal on the MNs. (Middle) Complementary DNA-210 imaged with 647ex/665em shows fluorescence signal bound to the MN. (Right) 3D projection of the fluorescence signal from a single microneedle. (Scale bar = 200μm).